Edge-On Self-Assembly of Tetra-bromoanthracenyl-porphyrin on Silver Surfaces

Nataliya Kalashnyk, Michel Daher Mansour, Joffrey Pijeat, Rémi Plamont, Xavier Bouju, Teodor Silviu Balaban, Stéphane Campidelli, Laurence Masson, Sylvain Clair

Edge-On Self-Assembly of Tetra-bromoanthracenyl-porphyrin on Silver Surfaces

Nataliya Kalashnyk,[#] Michel Daher Mansour,[#] Joffrey Pijeat, Rémi Plamont, Xavier Bouju, Teodor Silviu Balaban, Stéphane Campidelli, Laurence Masson, and Sylvain Clair*

Molecular self-assembly on surfaces is driven by the range of interactions between the molecules themselves and the substrate. Generally, a face-on structure is favored for aromatic molecules lying !at on the surface. Here, we report on the supramolecular self-assembly of 5,10,15,20-tetrakis(10-bromoanthracen-9-yl)porphyrin on the Ag(111) and Ag(110) surfaces. Well-ordered molecular chains were observed by room-temperature scanning tunneling microscopy on both surfaces. The relatively small size of the unit cell revealed an edge-on con"guration of the porphyrin macrocycles, that is, perpendicular to the surface plane, as confirmed by molecular mechanics calculations. Distinct intermolecular interactions were found on the two surfaces, providing different molecular chain orientations on Ag(111) and Ag(110).

The control on the structure of supramolecular architectures on a surface is of prime importance to steer their properties.[1−3] For two-dimensional (2D) self-assemblies in a monolayer or submonolayer regime, conformational adaptation is often produced as a response to various stimuli and a transition from 2D planar to three-dimensional (3D) reticular geometry can be observed.[4−7] Porphyrins are a widely studied class of molecules exhibiting promising electronic, optical, magnetic, or catalytic properties with large interest in materials science for many applications.[8−11] Porphyrin-based thin films deposited on a solid surface can be easily processed and investigated at the molecular level by scanning probe microscopy techniques.[12−14] They most generally adopt a face-on conformation to optimize their adsorption on a metal or a HOPG surface, but an edge-on geometry can also be observed because of the presence and the size of side groups, the nature of the solvent, or the concentration.[15−20] The edge-on self-assembly is particularly attractive because it allows for charge migration along the columnar structure,[21] thus providing particular mesoscopic properties appealing for molecular electronics. More elaborated strategies based on the use of a self-assembled monolayer (SAM) as a support have also been implemented to gain advanced control on the self-assembly of porphyrins.[22,23]

Tetra-anthracenylporphyrin (**TAP**) derivatives were first studied for their particular bis-facially blocked geometries because of the perpendicular anthracenyl groups and were tested as catalysts for the reversible coordination of oxygen,[24] the oxidation of PAHs,[25] or as active molecules against HIV infection.[26] From a synthetic point of view, the formation of

Nataliya Kalashnyk − *Aix Marseille Univ, Université de Toulon, CNRS, IM2NP, Marseille, France*
Michel Daher Mansour − *Aix Marseille Univ, CNRS, CINAM, Marseille, France*
Joffrey Pijeat − *Université Paris-Saclay, CEA, CNRS, NIMBE, LICSEN, 91191 Gif-sur-Yvette, France*
Rémi Plamont − *Aix Marseille Univ, CNRS, Centrale Marseille, ISM2, Marseille, France*
Xavier Bouju − *CEMES-CNRS, Université de Toulouse, 31055 Toulouse, France;* orcid.org/0000-0001-7827-3496
Teodor Silviu Balaban − *Aix Marseille Univ, CNRS, Centrale Marseille, ISM2, Marseille, France*
Stéphane Campidelli − *Université Paris-Saclay, CEA, CNRS, NIMBE, LICSEN, 91191 Gif-sur-Yvette, France;* orcid.org/0000-0001-6060-4891
Laurence Masson − *Aix Marseille Univ, CNRS, CINAM, Marseille, France*

TAP derivatives is a challenge.[27−29] **TAP** was first synthetized by Cense et al.[24] in 1979 following the method developed by Adler and Longo and the porphyrin was isolated in 0.2% yield.[30] Thereafter, attempts to synthesize **TAP** using the Lindsey strategy[31] or the reaction in inorganic acid[32] were reported and barely reached 3% yield. In 1985, Volz and Schaeffer reported a new synthetic method based on the formation of a pyrrole-carbinol intermediate, which cyclotetramerized in propionic acid to form **TAP** in 6% yield.[33] The strategy of Volz and Schaeffer was also applied by the group of Anderson in 2010 to synthetize a tetra-dimesityloxyanthracenylporphyrin in 10% yield and by Filatov et al.[34] in 2015 to synthesize a tetraphenylanthracenyl porphyrin in 15% yield. The symmetry matching between the anthracene moieties and the macrocycle of porphyrins was exploited by the group of Anderson to form a π-extended porphyrin exhibiting a maximum absorption around 1400 nm after the fusion of the four dimesityloxyanthracene groups on the porphyrin core.[35] Recently, we reported the synthesis of 5,10,15,20-tetrakis(10-bromoanthracen-9-yl)porphyrin (**TBAP**, Figure 1a and synthetic details in Supporting Information Figure S1) and we demonstrated its successful reactivity in Suzuki−Miyaura cross-coupling reactions.[36]

Here, we tackled the adsorption of **TBAP** on silver surfaces with a longer-term goal to create elaborated supramolecular or covalent 2D superstructures with this original precursor. Indeed, halogenated porphyrins have recently attracted attention for their ability to create a robust nanostructure in an on-surface synthesis approach.[2,37−39] We focused on the influence of the large bromoanthracenyl groups on the self-assembly processes directed by a well-defined metal surface. More precisely, we selected the Ag(111) and Ag(110) surfaces (Figure 1b) for their mild reactivity and their two distinct crystallographic structures.

Methods

The **TBAP** molecules were obtained from PorphyChem company (https://www.porphychem.com) or synthesized following the literature procedure (see Supporting Information, Figure S1).[36]

The STM experiments were performed in ultrahigh vacuum (UHV, base pressure in the 10^{-10} mbar range) in two different experimental setups. The single-crystal Ag(111) and Ag(110) surfaces were cleaned by several cycles of Ar^+ bombardment,

followed by annealing. The precursors were thoroughly degassed prior to deposition onto the atomically clean substrate. STM measurements were performed at room temperature with a commercial Omicron VT-STM system. The STM images were acquired in constant current mode with typical tunneling current $I_T \approx 0.1-0.3$ nA and sample bias $V_T \approx \pm(1-1.5)$ V. All images were subsequently calibrated using atomically resolved images of the pristine surfaces with an accuracy of ±5%. Images were partly treated with the free WSxM[40] and Gwyddion[41] software programs.

Molecular mechanics calculations were performed using a numerical code based on the atom superposition and electron delocalization (ASED-MO) method[42,43] with an extension including dispersive interactions to account for the long-range intermolecular forces (ASED+).[44] A semiempirical approach with the extended Hückel molecular orbital theory constitutes the core of the ASED-MO method. The so-called ASED+ code is a powerful numerical tool to describe reasonably well the structural properties of various types of molecules adsorbed on surfaces or in the gas phase.[45−47]

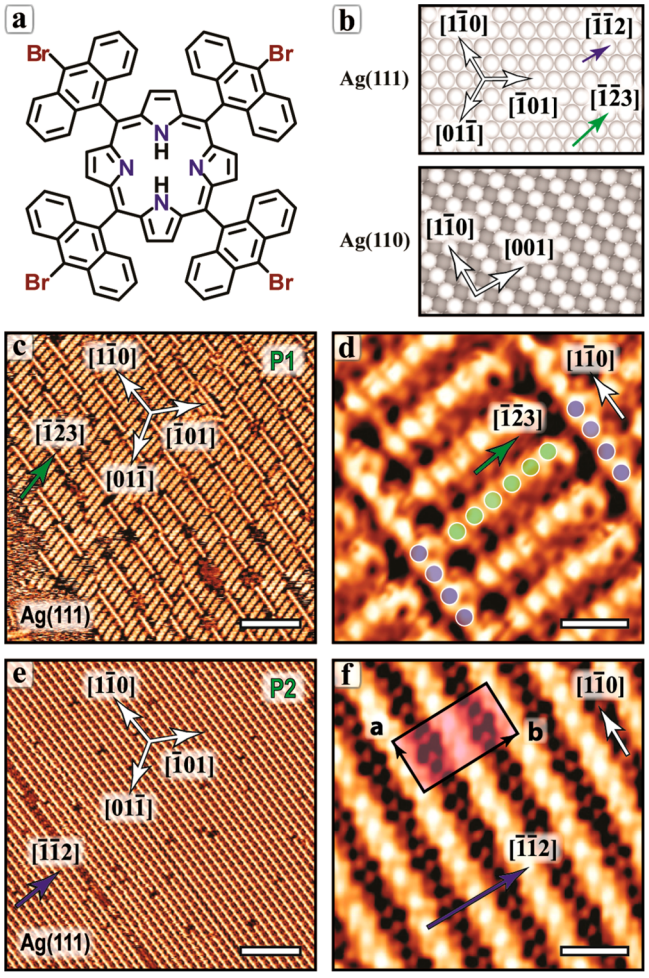

Figure 1. Schematic drawing of the (a) **TBAP** molecule and (b) Ag(111) and Ag(110) surfaces. (c) STM image of the self-assembly of **TBAP** on Ag(111) after room-temperature deposition (P1 phase) and (d) corresponding zoomed-in image. (e) P2 phase obtained after annealing at 200 °C and (f) corresponding zoomed-in image. The unit cell is indicated in (f) with a = 1.4 nm and b = 3.0 nm. Scale bars (c,e) 12 nm and (d,f) 2 nm.

Results and discussion

The deposition of **TBAP** on Ag(111) at room temperature leads to the formation of supramolecular domains corresponding to phase P1 as shown in Figure 1c. This phase consists in straight molecular chains with two distinct nearly orthogonal orientations. Most of the chains are aligned along the $[\bar{1}\,\bar{2}\,3]$ direction of the substrate and are about 5 nm long. The periodicity inside a chain is 0.8 nm (green dots in Figure 1d). The chains are regularly distributed distanced 1.4 nm between two adjacent chains, thus the interchain spacing corresponds to 5 substrate atomic distances along the $[1\bar{1}0]$ direction. As shown in the high-resolution STM image in Figure 1d, these molecular chains have locally a well-defined length, and they are stacked together and packed between perpendicularly positioned chains, which are 5 to 10 nm long (blue dots in Figure 1d, aligned along the $[1\bar{1}0]$ direction). Along these $[1\bar{1}0]$-chains, the periodicity is 0.7 nm, thus corresponding to a 2.5 substrate atomic distance. A tentative epitaxial model for the STM image in Figure 1d is reported in Supporting Information, Figure S2a. The similar periodicities along both chain types suggest a unique intermolecular configuration in phase P1.

Upon annealing at 200 °C, the self-assembly evolves into long molecular chains aligned with the $[1\bar{1}0]$ direction of the silver substrate and extends up to 100 nm or more (phase P2, Figure 1e). The interchain distance is 1.5 nm. In fact, here the periodic unit along the chain direction (**a** vector) comprises two molecules. This can be more clearly seen in some STM images acquired with a particular tip state and exhibiting a different contrast, as shown, for example, in Supporting Information Figure S3. This consistently produces an epitaxial relationship of 5 substrate atomic distances along the $[1\bar{1}0]$ direction (see Supporting Information Figure S2b for a tentative epitaxial model). The average intermolecular spacing (or half of the unit cell **a**) is 0.7 nm and the long intermolecular distance is about 4% larger while the short one is ~4% shorter. In addition, every second chain is slightly shifted along the $[1\bar{1}0]$ direction so that the unit cell includes two neighboring chains (**b** vector, aligned with the $[\bar{1}\,\bar{1}\,2]$ direction).

The small periodicity (<1 nm) along the molecular chains is not compatible with a flat-lying adsorption of the porphyrins.

Indeed, the 4 Br atoms in the molecule form a square pattern 1.4 nm wide (Figure 2a) with a size compatible with the

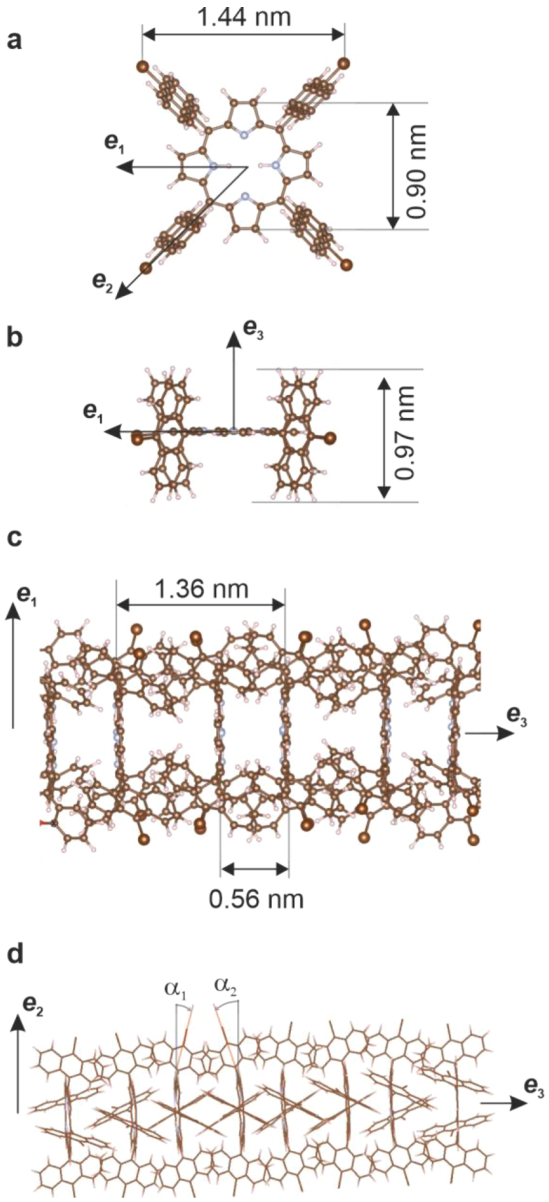

Figure 2. Molecular mechanics calculations. (a,b) Structure of the relaxed isolated **TBAP** molecule. (c,d) Gas-phase columnar structure. A dimerization of the porphyrin cores is obtained, while the distance between the anthracenyl planes is kept constant. The C−Br bond of the bromoanthracenyl groups is alternatively tilted by an angle α_1 = 8.2° and α_2 = −9.5°.

interchain spacing (1.5 nm) but not with the average intermolecular spacing (0.7 nm). To elucidate the supramolecular configuration of the chain structure, we performed gas-phase molecular mechanics calculations of a **TBAP** columnar structure for which the porphyrin macrocycle plane was set parallel for all molecules and perpendicular to the chain direction associated with the e_3 molecular axis (see Figure 2a–c). In this way, the anthracenyl groups could adequately rotate to create π-stacking interaction between the molecular units. We found an average optimum distance between two neighboring porphyrin cycles of 0.68 nm, in good agreement

with the experimental results. For comparison, the ideal $\pi-\pi$ stacking distance in a columnar porphyrin crystal is close to 0.4 nm,[48] while a stacking distance of 0.4−0.7 nm was observed in the edge-on self-assembly of other metal-free[16,18] or metallo-porphyrin[17,20,21,49] derivatives.

The calculations revealed a tendency for the molecules to dimerize by locally adjusting the distance between the porphyrin planes. As a result, within a dimer, the neighboring porphyrin cores are located 0.56 nm apart. Remarkably, in this structure, the distance between the anthracenyl planes remains rather constant (0.35 nm). This is obtained thanks to a distortion of the C−C bonds joining the anthracenyl group to the porphyrin macrocycle, inducing a slight in-plane rotation alternatively to the one or to the other end of the columnar structure (Figure 2d). The structure and the size of the modeled structure are thus in good agreement with the experimental results on the Ag(111) surface, with the e_3 axis of the molecule aligned with the $[1\bar{1}0]$ direction, that is, the chain direction. Furthermore, the tendency to dimerize observed in the gas-phase simulation is compatible with the fact that there are two molecules per unit cell in the supramolecular phase as measured by STM.

To modulate the molecule−substrate interaction, we performed additional deposition experiments on the open Ag(110) surface. Similarly, an ordered structure was found after room-temperature deposition, consisting mainly in short chains, 3 or 4 nm in length, aligned along the $[1\bar{1}0]$ substrate direction (phase P3, Figure 3a,b). The terminations of the chains are systematically aligned with the perpendicular [001] direction, indicating an important interchain interaction at the chain endings.

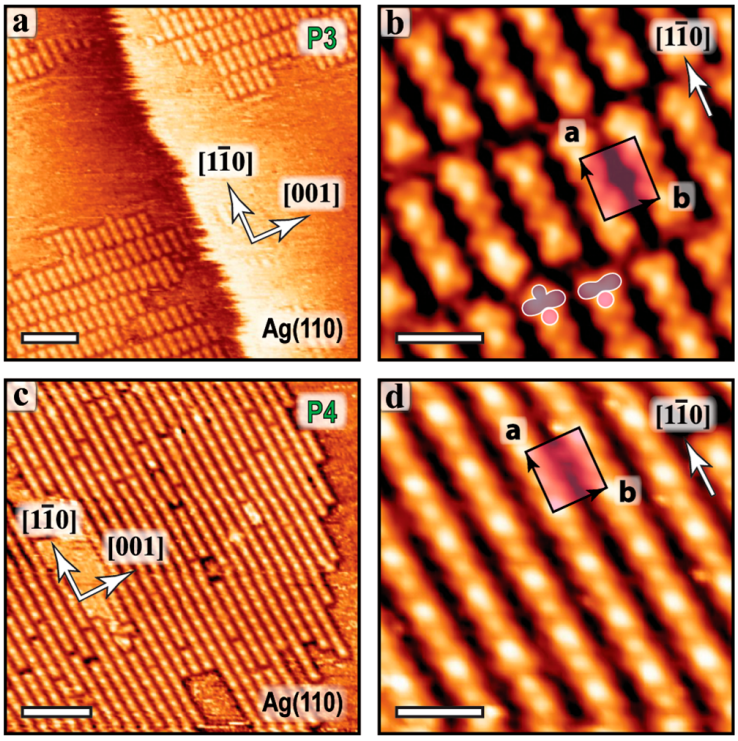

Figure 3. STM images of the self-assembly of **TBAP** on Ag(110). (a) After room-temperature deposition (P3 phase). (b) Corresponding zoomed-in image. The chain endings are imaged with either a concave or a convex shape, as highlighted by the purple cartoon in the bottom of the image. (c) P4 phase obtained after annealing to 300 °C. (d) Corresponding zoomed-in image. The unit cell is a = 1.4 nm and b = 1.2 nm. Scale bars (a,c) 7 nm, (b,d) 2 nm.

Upon deposition at 300 °C, the chains markedly elongate and can reach 40 nm in length (Figure 3c,d). The periodicity along the chains is 1.4 nm and corresponds to 5 substrate atomic distances along the $[1\bar{1}0]$ direction. The parallel chains are located 1.2 nm apart, corresponding to 3 substrate atomic distances along the [001] direction (see Supporting Information Figure S2c for a tentative epitaxial model).

Here again, we can exclude a flat-lying configuration because of the small size of the unit cell. However, the interchain distance is significantly shorter than in P1 and P2 phases on Ag(111) (1.2 nm vs 1.4 nm), so that the columnar structure is also not compatible. Rather, the side extension of **TBAP** (1.44 nm, Figure 2a) is consistent with the periodicity along the chain direction (**a** in Figure 3d, 1.4 nm). In fact, this distance is very close to the interchain distance in phase P2 on Ag(111). We thus suggest a molecular model where the porphyrin macrocycle plane is aligned with the chain direction (with the e_3 axis of **TBAP** perpendicular to $[1\bar{1}0]$, i.e., the chain direction). Consequently, the STM contrasts along the chains have completely different origins on the two surfaces. Figure 4

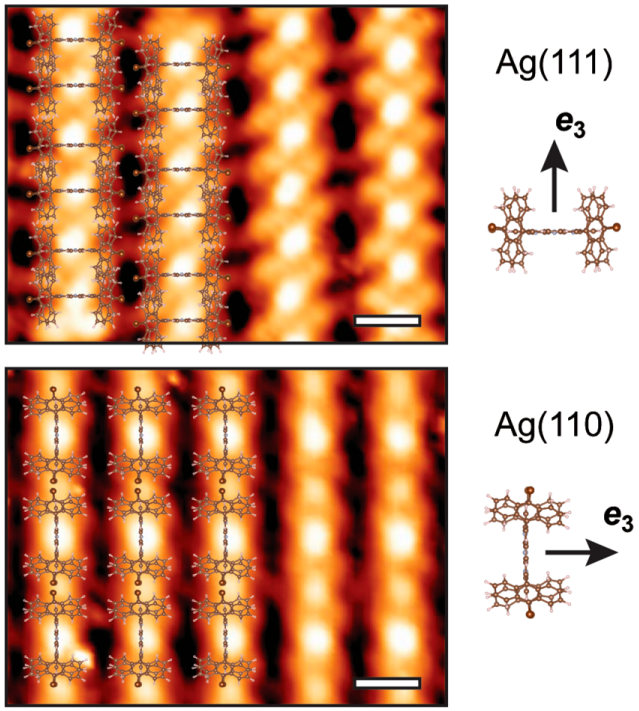

Figure 4. Comparison of the intermolecular configurations on Ag(111) and Ag(110). The tentative molecular models are superimposed on STM images. Scale bars: 1 nm.

shows that the apparent contrast of the chain formation is aligned with (or perpendicular to) the porphyrin planes on Ag(110) (or Ag(111)), respectively. We excluded the possibility of a tilted configuration (with the e_3 axis neither aligned nor perpendicular to the chain direction) because of the high symmetry of the STM contrast with respect to the chain direction. The particularity of the P3/P4 phases on Ag(110) consists in the longer distance between the molecules in the columnar direction (e_3 axis) for which no favorable $\pi-\pi$ interaction between the anthracenyl groups is allowed. If we consider the epitaxial interaction as the main driving force for the self-assembly, a denser (5 × 2) superstructure (instead of the observed (5 × 3) structure) would produce an intermolecular distance between the porphyrin planes of 0.8 nm, slightly different from what is observed in P1 and P2 (0.7 nm). It is suggested that a different adsorption configuration and a different conformation of the rotating anthracenyl groups

is responsible for this behavior. Noteworthily, the strength of the intermolecular interaction along [001] (e_3 axis) is sufficiently strong so that extended well-ordered chains are formed. This is particularly demonstrated in phase P3 for which all chain endings are perfectly aligned. The fact that short chains are found after room-temperature deposition on both Ag(111) and Ag(110) surfaces suggests a rather strong interaction of the molecules with the silver surfaces. The elongation of the chains after annealing may be facilitated by the increase of diffusivity at higher temperature, but it is also possibly activated by a conformational (rotation of anthracenyl) or chemical (loss of Br) change.

After room-temperature deposition on Ag(110), we also found another phase (phase P5, Figure 5), with large well-

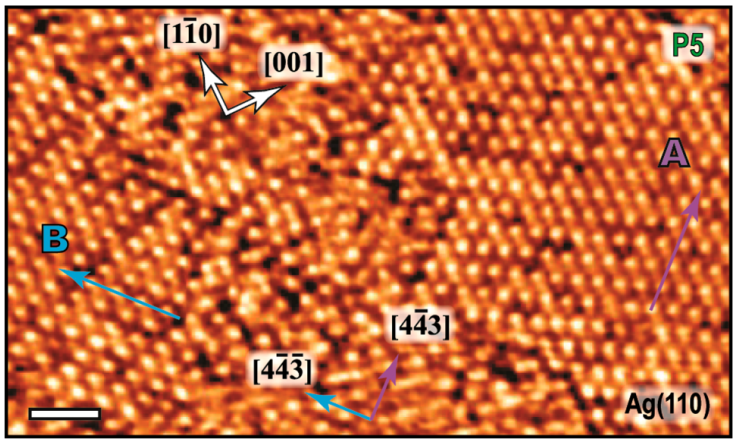

Figure 5. STM image of the metastable domains (phase P5) obtained on Ag(110) after room-temperature deposition. A and B are mirror symmetric. Scale bar: 5 nm.

organized domains and coexisting with phase P3. This metastable phase disappeared upon slight annealing at 100 °C. The structure here is still composed of molecular chains aligned along the [1$\bar{1}$0] direction but with a rhombic pattern. The periodicity along the [1$\bar{1}$0] direction is of 6 substrate atomic distances, that is 20% larger than in phase P3, but the periodicity of the molecular chains along the [001] direction remains the same, that is, 1.2 nm (3 substrate atomic distances) (see Supporting Information Figure S2d). In these domains, the **TBAP** molecules have the same orientation as in P3 and P4, but they are simply positioned further apart along their e_1 axis and not any more aligned along the [001] direction. Two kinds of rhombic domains are observed (labeled A and B in Figure 5), depending on the porphyrin core shift between two adjacent chains of ±2 substrate atomic distances along [1$\bar{1}$0]. The formation of ordered 2D domains confirms the presence of substantial intermolecular interactions along [1$\bar{1}$0] and also in the other domain high-symmetry directions.

Finally, it should be noted that in the high-resolution images of phase P3, the apparent contrast at the chain termination is randomly distributed with either a concave or a convex shape (as highlighted in Figure 3b). This may indicate a partial dehalogenation of the molecules. Therefore, rather than halogen bonding,[50] the formation of metal−organic links along the apparent chain direction through insertion of Ag adatoms cannot be excluded on Ag(110), similar to what is usually observed for halogenated precursors on various metal surfaces.[2,51−53] This issue could also explain the observation of the rhombic metastable phase P5, composed of longer chains at room temperature but with larger intermolecular distances

along the chain direction, for which the metal−organic bonding would not be achieved yet.

CONCLUSIONS

We studied the self-assembly of **TBAP** molecules on the Ag(111) and Ag(110) surfaces. The molecules adopt an edge-on configuration and form extended 2D domains of highly ordered chains after annealing. The formation of the chains originates from two distinct processes on theses surfaces. On Ag(111), a columnar structure is formed through $\pi-\pi$ interaction between the anthracenyl groups. On Ag(110), the chains are formed through lateral interaction between the molecules, possibly aided by the formation of metal−organic complexes. The **TBAP** precursor can adopt different 3D configurations because of the many degrees of liberty gained by the frustrated rotation of the four bromoanthracenyl groups. As a result, radically different intermolecular interactions can take place, leading to important modifications in the supramolecular organization. Accordingly, noticeable variations in their overall properties can be expected.[8,11] Our results should provide inspiration for a guided and modular complex 2D self-assembly on a surface by taking use of a single intrinsically three-dimensional functional precursor.

Acknowledgments

L. Nony and F. Bocquet are gratefully acknowledged for their support in image treatment. This work was partly funded by the ANR program project MAGMA (ANR-16-CE29-0027-01) and by a public grant overseen by the French National Research Agency (ANR) as part of the "Investissements d'Avenir" program (Labex NanoSaclay, reference: ANR-10-LABX-0035).

References

(1) Barth, J. V.; Costantini, G.; Kern, K. Engineering Atomic and Molecular Nanostructures at Surfaces. *Nature* **2005**, *437*, 671.
(2) Clair, S.; De Oteyza, D. G. Controlling a Chemical Coupling Reaction on a Surface: Tools and Strategies for On-Surface Synthesis. *Chem. Rev.* **2019**, *119*, 4717−4776.
(3) Bouju, X.; Mattioli, C.; Franc, G.; Pujol, A.; Gourdon, A. Bicomponent Supramolecular Architectures at the Vacuum-Solid Interface. *Chem. Rev.* **2017**, *117*, 1407−1444.
(4) Klappenberger, F.; Cañas-Ventura, M. E.; Clair, S.; Pons, S.; Schlickum, U.; Qu, Z.-R.; Brune, H.; Kern, K.; Strunskus, T.; Wöll, C.; et al. Conformational Adaptation in Supramolecular Assembly on Surfaces. *ChemPhysChem* **2007**, *8*, 1782−1786.
(5) Schultz, J. F.; Li, L.; Mahapatra, S.; Shaw, C.; Zhang, X.; Jiang, N. Defining Multiple Configurations of Rubrene on a Ag(100) Surface with 5 angstrom Spatial Resolution via Ultrahigh Vacuum Tip-Enhanced Raman Spectroscopy. *J. Phys. Chem. C* **2020**, *124*, 2420−2426.
(6) Vogt, M.; Buschmann, R.; Toksabay, S.; Schmitt, M.; Schwab, M.; Bode, M.; Krueger, A. Self-Assembly and Electronic Structure of Tribenzotriquinacenes on Ag(111). *J. Phys. Chem. C* **2019**, *123*, 5469−5478.
(7) Kalashnyk, N.; Dumur, F.; Gigmes, D.; Clair, S. Molecular adaptation in supramolecular self-assembly: brickwall-type phases of indacene-tetrone on silver surfaces. *Chem. Commun.* **2018**, *54*, 8510−8513.
(8) Smykalla, L.; Mende, C.; Fronk, M.; Siles, P. F.; Hietschold, M.; Salvan, G.; Zahn, D. R. T.; Schmidt, O. G.; Rüffer, T.; Lang, H. (Metallo)porphyrins for potential materials science applications. *Beilstein J. Nanotechnol.* **2017**, *8*, 1786−1800.
(9) Kuzmin, S. M.; Chulovskaya, S. A.; Parfenyuk, V. I. Structures and Properties of Porphyrin-Based Film Materials Part I. The Films Obtained via Vapor-Assisted Methods. *Adv. Colloid Interface Sci.* **2018**, *253*, 23−34.
(10) Chilukuri, B.; Mazur, U.; Hipps, K. W. Structure, Properties, and Reactivity of Porphyrins on Surfaces and Nanostructures with Periodic DFT Calculations. *Appl. Sci.* **2020**, *10*, 740.
(11) Diercks, C. S.; Lin, S.; Kornienko, N.; Kapustin, E. A.; Nichols, E. M.; Zhu, C.; Zhao, Y.; Chang, C. J.; Yaghi, O. M. Reticular Electronic Tuning of Porphyrin Active Sites in Covalent Organic Frameworks for Electrocatalytic Carbon Dioxide Reduction. *J. Am. Chem. Soc.* **2018**, *140*, 1116−1122.
(12) Gottfried, J. M. Surface Chemistry of Porphyrins and Phthalocyanines. *Surf. Sci. Rep.* **2015**, *70*, 259−379.
(13) Auwärter, W.; Écija, D.; Klappenberger, F.; Barth, J. V. Porphyrins at Interfaces. *Nat. Chem.* **2015**, *7*, 105−120.
(14) Otsuki, J. STM Studies on Porphyrins. *Coord. Chem. Rev.* **2010**, *254*, 2311−2341.
(15) El Garah, M.; Santana Bonilla, A.; Ciesielski, A.; Gualandi, A.; Mengozzi, L.; Fiorani, A.; Iurlo, M.; Marcaccio, M.; Gutierrez, R.; Rapino, S.; et al. Molecular Design Driving Tetraporphyrin Self-Assembly on Graphite: a Joint STM, Electrochemical and Computational Study. *Nanoscale* **2016**, *8*, 13678−13686.
(16) Adachi, K.; Hirose, T.; Matsuda, K. The Polymorphism of Porphyrin 2D Assemblies at the Liquid-Graphite Interface: the Effect of a Polar Solvent Additive and a Flexible Spacer on the Face-On and

Edge-On Type Molecular Arrangements. *Chem. Commun.* **2019**, *55*, 8836−8839.
(17) Sakano, T.; Hasegawa, J.-y.; Higashiguchi, K.; Matsuda, K. Chronological Change from Face-On to Edge-On Ordering of Zinc-Tetraphenylporphyrin at the Phenyloctane-Highly Oriented Pyrolytic Graphite Interface. *Chem. Asian J.* **2012**, *7*, 394−399.
(18) Otsuki, J.; Namiki, K.; Arai, Y.; Amano, M.; Sawai, H.; Tsukamoto, A.; Hagiwara, T. Face-on and Columnar Porphyrin Assemblies at Solid/Liquid Interface on HOPG. *Chem. Lett.* **2009**, *38*, 570−571.
(19) Trelka, M.; Urban, C.; Rogero, C.; de Mendoza, P.; Mateo-Marti, E.; Wang, Y.; Silanes, I.; Écija, D.; Alcamí, M.; Yndurain, F.; et al. Surface Assembly of Porphyrin Nanorods with One-Dimensional Zinc-Oxygen Spinal Cords. *CrystEngComm* **2011**, *13*, 5591−5595.
(20) Zhou, Y.; Wang, B.; Zhu, M.; Hou, J. G. Observation of Co-Existence of 'Face-On' and 'Edge-On' Stacking Styles in a Porphyrin Monolayer. *Chem. Phys. Lett.* **2005**, *403*, 140−145.
(21) Schouten, P. G.; Warman, J. M.; de Haas, M. P.; Anne Fox, M.; Pan, H.-L. Charge Migration in Supramolecular Stacks of Peripherally Substituted Porphyrins. *Nature* **1991**, *353*, 736−737.
(22) Lombana, A.; Battaglini, N.; Tsague-Kenfac, G.; Zrig, S.; Lang, P. In-Solution Patterning of Standing Up Porphyrin Based Nanostructures within Hydrogen Bonded Porous Networks - a Structural Effect of a Host Matrix on Guest Entities. *Chem. Commun.* **2016**, *52*, 5742−5745.
(23) Otte, F. L.; Lemke, S.; Schütt, C.; Krekiehn, N. R.; Jung, U.; Magnussen, O. M.; Herges, R. Ordered Monolayers of Free-Standing Porphyrins on Gold. *J. Am. Chem. Soc.* **2014**, *136*, 11248−11251.
(24) Cense, J.-M.; Le Quan, R.-M. Oxygenation d'une ferroporphyrine encombree sur ses deux faces, la ferromeso-tetra-anthracenyl phorphine. *Tetrahedron Lett.* **1979**, *20*, 3725−3728.
(25) Harden, G. J.; Coombs, M. M. Biomimetic iron porphyrin-catalysed oxidation of cyclopenta [a] phenanthrenones. *J. Chem. Soc., Perkin Trans. 1* **1995**, 3037−3042.
(26) Vzorov, A. N.; Dixon, D. W.; Trommel, J. S.; Marzilli, L. G.; Compans, R. W. Inactivation of human immunodeficiency virus type 1 by porphyrins. *Antimicrob. Agents Chemother.* **2002**, *46*, 3917−3925.
(27) Sooambar, C.; Troiani, V.; Bruno, C.; Marcaccio, M.; Paolucci, F.; Listorti, A.; Belbakra, A.; Armaroli, N.; Magistrato, A.; De Zorzi, R.; et al. Synthesis, photophysical, electrochemical, and electrochemiluminescent properties of 5,15-bis(9-anthracenyl)porphyrin derivatives. *Org. Biomol. Chem.* **2009**, *7*, 2402−2413.
(28) Davis, N. K. S.; Thompson, A. L.; Anderson, H. L. Bis-Anthracene Fused Porphyrins: Synthesis, Crystal Structure, and Near-IR Absorption. *Org. Lett.* **2010**, *12*, 2124−2127.
(29) Davis, M.; Senge, M. O.; Locos, O. B. Anthracenylporphyrins. *Z. Naturforsch. B Chem. Sci.* **2010**, *65*, 1472−1484.
(30) Adler, A. D.; Longo, F. R.; Shergalis, W. Mechanistic Investigations of Porphyrin Syntheses. I. Preliminary Studies on ms-Tetraphenylporphin. *J. Am. Chem. Soc.* **1964**, *86*, 3145−3149.
(31) Tohara, A.; Sato, M. An improved synthesis of meso-tetraanthryiporphyrin by a kinetically controlled Lindsey reaction. *J. Porphyr. Phthalocyanines* **2007**, *11*, 513−518.
(32) Kumar, A.; Maji, S.; Dubey, P.; Abhilash, G. J.; Pandey, S.; Sarkar, S. One-pot general synthesis of metalloporphyrins. *Tetrahedron Lett.* **2007**, *48*, 7287−7290.
(33) Volz, H.; Schaeffer, H. Mesosubstituted Porphyrins. III. 5,10,15,20-Tetraanthracenylporphyrin. *Chem. Ztg.* **1985**, *109*, 308−309.
(34) Filatov, M. A.; Heinrich, E.; Busko, D.; Ilieva, I. Z.; Landfester, K.; Baluschev, S. Reversible oxygen addition on a triplet sensitizer molecule: protection from excited state depopulation. *Phys. Chem. Chem. Phys.* **2015**, *17*, 6501−6510.
(35) Davis, N. K. S.; Thompson, A. L.; Anderson, H. L. A Porphyrin Fused to Four Anthracenes. *J. Am. Chem. Soc.* **2011**, *133*, 30−31.
(36) Pijeat, J.; Dappe, Y. J.; Thuéry, P.; Campidelli, S. Synthesis and Suzuki-Miyaura Cross Coupling Reactions for Post-Synthetic

Modification of a Tetrabromo-Anthracenyl Porphyrin. *Org. Biomol. Chem.* **2018**, *16*, 8106−8114.
(37) Grill, L.; Dyer, M.; Lafferentz, L.; Persson, M.; Peters, M. V.; Hecht, S. Nano-Architectures by Covalent Assembly of Molecular Building Blocks. *Nat. Nanotechnol.* **2007**, *2*, 687−691.
(38) Ferreira, R. C. D.; Paz, A. P.; Mowbray, D. J.; Roulet, J. Y.; Landers, R.; de Siervo, A. Supramolecular Ordering and Reactions of a Chlorophenyl Porphyrin on Ag(111). *J. Phys. Chem. C* **2020**, *124*, 14220−14228.
(39) Sen, D.; Błoński, P.; Torre, B. d. l.; Jelínek, P.; Otyepka, M. Thermally induced intra-molecular transformation and metalation of free-base porphyrin on Au(111) surface steered by surface confinement and ad-atoms. *Nanoscale Adv.* **2020**, *2*, 2986−2991.
(40) Horcas, I.; Fernández, R.; Gómez-Rodríguez, J. M.; Colchero, J.; Gómez-Herrero, J.; Baro, A. M. WSXM: A software for scanning probe microscopy and a tool for nanotechnology. *Rev. Sci. Instrum.* **2007**, *78*, 013705.
(41) Necas, D.; Klapetek, P. Gwyddion: an open-source software for SPM data analysis. *Cent. Eur. J. Phys.* **2012**, *10*, 181−188.
(42) Anderson, A. B. Electron density distribution functions and the ASED −MO theory. *Int. J. Quantum Chem.* **1994**, *49*, 581−589.
(43) Bosson, M.; Richard, C.; Plet, A.; Grudinin, S.; Redon, S. Interactive quantum chemistry: A divide-and-conquer ASED-MO method. *J. Comput. Chem.* **2012**, *33*, 779−790.
(44) Ample, F.; Joachim, C. A semi-empirical study of polyacene molecules adsorbed on a Cu(110) surface. *Surf. Sci.* **2006**, *600*, 3243−3251.
(45) Perera, U. G. E.; Ample, F.; Kersell, H.; Zhang, Y.; Vives, G.; Echeverria, J.; Grisolia, M.; Rapenne, G.; Joachim, C.; Hla, S.-W. Controlled clockwise and anticlockwise rotational switching of a molecular motor. *Nat. Nanotechnol.* **2013**, *8*, 46−51.
(46) Villagomez, C. J.; Guillermet, O.; Goudeau, S.; Ample, F.; Xu, H.; Coudret, C.; Bouju, X.; Zambelli, T.; Gauthier, S. Self-assembly of enantiopure domains: The case of indigo on Cu(111). *J. Chem. Phys.* **2010**, *132*, 074705.
(47) Makoudi, Y.; Duverger, E.; Arab, M.; Chérioux, F.; Ample, F.; Rapenne, G.; Bouju, X.; Palmino, F. Room-temperature electronic template effect of the SmSi(111)-8 x 2 interface for self-alignment of organic molecules. *ChemPhysChem* **2008**, *9*, 1437−1441.
(48) Castella, M.; Lopez-Calahorra, F.; Velasco, D.; Finkelmann, H. The first asymmetrically beta-polysubstituted porphyrin-based hexagonal columnar liquid crystal. *Chem. Commun.* **2002**, 2348−2349.
(49) Écija, D.; Auwärter, W.; Vijayaraghavan, S.; Seufert, K.; Bischoff, F.; Tashiro, K.; Barth, J. V. Assembly and Manipulation of Rotatable Cerium Porphyrinato Sandwich Complexes on a Surface. *Angew. Chem., Int. Ed.* **2011**, *50*, 3872−3877.
(50) Teyssandier, J.; Mali, K. S.; De Feyter, S. Halogen Bonding in Two-Dimensional Crystal Engineering. *ChemistryOpen* **2020**, *9*, 225−241.
(51) Galeotti, G.; Di Giovannantonio, M.; Lipton-Duffin, J.; Ebrahimi, M.; Tebi, S.; Verdini, A.; Floreano, L.; Fagot-Revurat, Y.; Perepichka, D. F.; Rosei, F.; et al. The Role of Halogens in On-Surface Ullmann Polymerization. *Faraday Discuss.* **2017**, *204*, 453−469.
(52) Barton, D.; Gao, H.-Y.; Held, P. A.; Studer, A.; Fuchs, H.; Doltsinis, N. L.; Neugebauer, J. Formation of Organometallic Intermediate States in On-Surface Ullmann Couplings. *Chem.—Eur. J.* **2017**, *23*, 6190−6197.
(53) Saywell, A.; Greń, W.; Franc, G.; Gourdon, A.; Bouju, X.; Grill, L. Manipulating the Conformation of Single Organometallic Chains on Au(111). *J. Phys. Chem. C* **2014**, *118*, 1719−1728.